Photoionization cross section for the 4s subshell of Zn I†

Arne W. Fliflet and Hugh P. Kelly
Department of Physics, University of Virginia, Charlottesville, Virginia 22901
(Received 26 December 1973)

We present a calculation of the photoionization cross section for the 4s subshell of neutral zinc using many-body perturbation theory. The cross section is strongly affected by correlations among 4s and 3d electrons. Resonances due to the $3d^9 4s^2 np$ configurations dominate the cross section and are split by the spin-orbit interaction. We have also included interactions between resonances. Correlations reduce the Hartree-Fock cross section by an order of magnitude near threshold. Our results are in qualitative agreement with the experimental data of Marr and Austin.

I. INTRODUCTION

The calculation of accurate photoionization cross sections for atoms near threshold provides a good indication of our understanding of atomic structures. As discussed in reviews by Fano and Cooper[1] and by Marr,[2] the photoionization cross section $\sigma(\omega)$ near threshold depends on aspects of the atomic system which are often not adequately represented by an independent-particle model. Methods for including many-body effects have recently been applied to the calculation of $\sigma(\omega)$ for the rare gases[3-6] and Fe I.[7] These calculations have demonstrated the importance of correlations among outer-shell electrons.

In this paper we present a calculation of $\sigma(\omega)$ for the 4s subshell of Zn I including correlations among the 4s and 3d electrons. The cross section for this atom is of particular interest because near threshold we find that the Hartree-Fock cross section differs by an order of magnitude from the experimental data of Marr and Austin.[8] In addition, their data for the 4s cross section is dominated by resonances which show large effects from spin-orbit splitting and it is interesting to test whether theory can reproduce this complex structure.

This calculation is based on the many-body perturbation theory (MBPT) of Brueckner[9] and Goldstone[10] and our techniques[11-13] for applying MBPT to atoms. We use the prescription for $\sigma(\omega)$ developed in Ref. 7 from the relation[1]

$$\sigma(\omega) = (4\pi/c)\,\omega\,\mathrm{Im}\,\alpha(\omega), \tag{1}$$

where $\alpha(\omega)$ is the frequency-dependent dipole polarizability[14,15] and c is the speed of light. Atomic units are used throughout unless otherwise noted. As is clear from Eq. (1), we consider only dipole radiation. We also neglect relativistic effects.

In Sec. II we give the theory with emphasis on new features of this calculation. These include the identification of diagrams in the expansion of $\sigma(\omega)$ which correspond to interactions between resonances and the modification of this expansion to include spin-orbit splitting of resonances. The formulation of $\sigma(\omega)$ in the region of an isolated resonance in terms of general MBPT quantities has been carried out by Wendin.[16] Section III contains an account of our calculations and numerical results. Section IV contains discussion of results and our conclusions.

II. THEORY

In previous work[7] a well-defined perturbation expansion for $\sigma(\omega)$ was obtained using Eq. (1) for an atom with Hamiltonian

$$H = \sum_{i=1}^{N}\left(-\tfrac{1}{2}\nabla_i^2 - \frac{Z}{r_1}\right) + \sum_{i<j=1}^{N} v_{ij}, \tag{2}$$

where v_{ij} is the Coulomb interaction between electrons. An expansion has also been obtained for the length (L) dipole matrix element

$$Z(p \to k) \equiv \langle \Psi(kp^{-1}) | \sum_i z_i | \Psi_0 \rangle, \tag{3}$$

where Ψ_0 and $\Psi(kp^{-1})$ are exact many-particle ground and continuum states and $\Psi(kp^{-1})$ results from the excitation of an electron from the ground-state orbital p to the excited-state orbital k. The velocity (V) form is obtained by replacing the matrix element in Eq. (3) by

$$\frac{1}{E_0 - E_k}\langle \Psi(kp^{-1}) | \sum_i \frac{d}{dz_i} | \Psi_0 \rangle,$$

where E_0 and E_k are energy eigenvalues corresponding to Ψ_0 and $\Psi(kp^{-1})$. Our continuum orbitals are normalized according to

$$R_k(r) \to (1/r)\cos[kr + (q/k)\ln(2kr) - \tfrac{1}{2}\pi(l-1) + \delta_l] \quad \text{as } r \to \infty, \tag{4}$$

where $V(r) \to q/r$. In this case[7]

$$\sigma(\omega) = (8\pi/c)\,N(\omega/k)\,|Z(p \to k)|^2, \tag{5}$$

where $k = [2(\omega - I)]^{1/2}$ with I the ionization energy and N a "normalization" factor (usually close to

unity) discussed below.

The matrix element $Z(p \to k)$ is obtained from the series of all open diagrams[7] with one dipole interaction and any number of interactions with the electron-correlation perturbation

$$H_c' = \sum_{i<j=1}^{N} v_{ij} - \sum_{i=1}^{N} V(r_i), \tag{6}$$

where $V(r_i)$ is the single-particle potential used to generate the single-particle orbitals. The order of interactions in the diagrams is from bottom to top corresponding to the ordering from right to left in the matrix element $Z(p \to k)$. Coulomb interactions before and after the dipole interaction contribute to ground-state correlations (GSC) and final-state correlations (FSC), respectively. Denominators occurring after the dipole interaction are shifted by $+\omega$ and are evaluated according to the rule

$$\lim_{\eta \to 0}(D + i\eta)^{-1} = PD - i\pi\delta(D),$$

where P stands for principal-value integration. Following Wendin,[16] in the diagrams we denote contributions of $-i\pi\delta(D)$ by a horizontal line. We have only included diagrams which occur in the random-phase approximation with exchange (RPAE).[3] Examples of these are shown in Figs. 1(a)–1(c). The RPAE also includes the corresponding exchange diagrams. Figure 1(d) shows a diagram not included in the RPAE. For closed-shell atoms, the m_l, m_s dependence of all diagrams ending in the hole-particle pair p, k with k in the state (m_l, m_s) is given by $C^1(l_k, m_l; l_p, m_l)$.[17,18] It is convenient to consider "reduced" diagrams which are obtained by factoring out this coefficient. Denoting the sum of the reduced diagrams by $Z_R(p \to k)$, the many-particle matrix element $Z(p \to k)$ is given by

$$Z(p \to k) = [A(l_k, l_p)]^{1/2} Z_R(p \to k), \tag{7}$$

where

$$A(l_k, l_p) = 2 \sum_{m_l=-l}^{l} [C^1(l_k, m_l; l_p, m_l)]^2. \tag{8}$$

In Eq. (8) the factor 2 comes from the sum over m_s (for a closed shell) and l equals the lesser of l_p and l_k.

The expansion for $Z(p \to k)$ does not include normalization diagrams[12]; and to lowest order, the contribution from these diagrams to $\sigma_{4s}(\omega)$ is included in the factor[12]

$$N = \left(1 + \sum_{q \neq 4s^+} N(4s^+, q)\right)^{-1}, \tag{9}$$

where $N(4s^+, q)$ represents the diagram shown in Fig. 1(e) and its exchange with squared denominator, and $4s^+$ denotes either one of the $4s$ electrons.

The diagrams are evaluated using complete sets of excited orbitals which are calculated using a Hartree-Fock (HF) V^{N-1} potential.[12] As discussed by Amus'ya *et al.*[3] and essentially by Ishihara and Poe,[19] the appropriate potential for orbitals excited by dipole transitions from a closed-shell ground state is obtained by coupling the excited orbital to the core to form a ^1P state. In the expansion of H_c', this potential cancels not only diagrams having interactions with passive unexcited states but also important intrashell correlation diagrams occurring in the RPAE.[3,19] The canceled diagrams include diagram 1(c) and its exchange when p and q are in the same subshell and k and k' have the same orbital angular momentum.

According to the MBPT prescription, the energy denominator occurring in the diagrams is given by

$$D = \sum_{i=1}^{N} (\mathcal{E}_{hi} - \mathcal{E}_{pi}) + \omega, \tag{10}$$

where $\mathcal{E}_{hi}$ and $\mathcal{E}_{pi}$ are single-particle energies for a hole (ground-state orbital) -particle (excited-state orbital) pair and N is the number of pairs excited. When D is a GSC denominator, ω is omitted. For clarity, consider the denominator of diagram 1(c) with $k' = nl$. Then we have

$$D = \mathcal{E}_q - \mathcal{E}_{nl} + \omega. \tag{11}$$

As discussed previously,[7,11,15,20] higher-order diagrams may be included by shifting denominator to $D' = D + \Delta(n)$, where $\Delta(n)$ includes the correlation energy of the nl orbital. In this calculation we have approximately included such effects by replacing $\mathcal{E}_q$ with minus the experimental removal

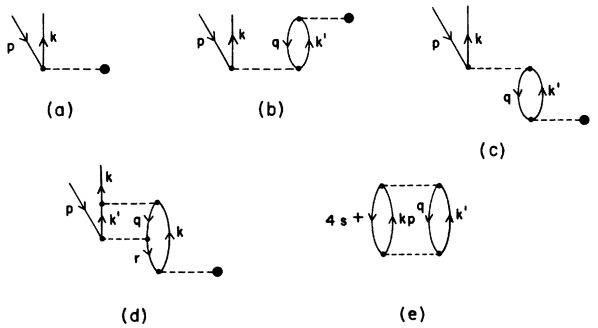

FIG. 1. Diagrams occurring in the perturbation expansion for $\langle \Psi(kp^{-1}) | \sum_i z_i | \Psi_0 \rangle$. Solid dots indicate matrix elements of z. Other dashed lines represent Coulomb interactions. Time increases upwards. Exchange diagrams are not shown. Diagram 1(e) is a normalization diagram and does not occur in the expansion for $\langle \Psi(kp^{-1}) | \sum_i z_i | \Psi_0 \rangle$.

energy of the q subshell, denoted by E_q. Excited orbital energies were taken to be HF calculated values. Using this procedure, Eq. (11) becomes exact, of course, for large n and gives photoionization thresholds correctly.

Bound configurations which may be excited via the dipole interaction and which are degenerate with the photoionization continuum configuration lead to resonances and will be referred to as resonance configurations. The possible resonance configurations for $\sigma_{4s}(\omega)$ for photon energies below the $3d$ ionization energy are $3d^9 4s^2 np\,{}^1P$ and $3d^9 4s^2 nf\,{}^1P$. We have neglected resonances due to the latter configurations since we find that the $3d \rightarrow nf$ matrix elements are very small. To calculate $Z(4s \rightarrow kp)$ we first consider all reduced diagrams not involving final-state correlations with resonance configurations $3d^9 4s^2 np\,{}^1P$. These diagrams are added to form a correlated direct transition matrix element $Z_R^D(4s \rightarrow kp)$ which is, in general, complex. The HF approximation, represented by diagram 1(a) with $p, k = 4s, kp$, is the lowest-order contribution to $\mathrm{Re}Z_R(4s \rightarrow kp)$. Higher-order contributions to $\mathrm{Re}Z_R(4s \rightarrow kp)$ are shown in Figs. 1(b) and 1(c) with $p, k = 4s, kp$ and in Figs. 3(a)–3(c). Diagram 1(c) with $p, k = 4s, kp$ and $q, k' = 3d, kp$ and kf contributes to $\mathrm{Im}Z_R^D(4s \rightarrow kp)$ when the denominator for q, k' is treated according to $-i\pi\delta(D)$. Diagram 2(b) with np replaced by kp and kf also contributes to $\mathrm{Im}Z_R(4s \rightarrow kp)$.

We next consider diagrams which include final-state correlations with the resonance configurations $3d^9 4s^2 np$. In the following discussion we begin by considering the case of no spin-orbit splitting and afterwards generalize our results. The lowest-order reduced resonance diagram which will be called RDI is shown in Fig. 1(c) with $p, k = 4s, kp$ and $q, k' = 3d, np$. This diagram has a series of simple poles from the sum over energy denominators

$$D_n(\omega) = E_{3d} - \mathcal{E}_{np} + \omega. \tag{12}$$

The poles are eliminated by including higher-order diagrams such as shown in Fig. 2(a) which together with RDI are the first two terms of a geometric series with ratio

$$R_G = -i \sum_m \frac{\frac{1}{2}\Gamma_m(\omega)}{D_m(\omega)}, \tag{13}$$

where

$$\tfrac{1}{2}\Gamma_m(\omega) = (2/k)\,|\langle \Phi_{kp}|v|\Phi_{mp}\rangle|^2. \tag{14}$$

In Eq. (14), v represents the Coulomb interaction and Φ_{kp} and Φ_{mp} are HF ^1P wave functions for the $3d^{10} 4s kp$ and $3d^9 4s^2 mp$ configurations. When $\omega = \mathcal{E}_{mp} - E_{3d}$, $\frac{1}{2}\Gamma_m$ is the half-width of the $3d^9 4s^2 mp\,{}^1P$ state. The diagram segment which contributes to R_G is shown in Fig. 2(c). The sum over m in R_G accounts for interactions between resonances. If these interactions may be neglected, $m = n$ in diagram 2(a) and the ratio reduces to one term. This is the imaginary part of the ratio used in the previous calculation for Ar I.[4] When $m = n$, the ratio may also be obtained from diagram segments of the form shown in Fig. 2(d) where both real and imaginary contributions from the denominator for the $4s \rightarrow kp$ excitation are included. Summing the series with this ratio yields RDI with shifted denominator[4]

$$D_n'(\omega) = D_n(\omega) - \Delta_n(\omega) + \tfrac{1}{2} i \Gamma_n(\omega), \tag{15}$$

where

$$\Delta_n(\omega) = \frac{2}{\pi}\,\mathrm{P}\int dk\, \frac{|\langle \Phi_{kp}|v|\Phi_{np}\rangle|^2}{E_{4s} - E_{kp} + \omega}, \tag{16}$$

and $\Delta_n(\omega)$ is a resonance energy shift due to interaction with the continuum which comes from the principal-value part of diagram segment 2(d). Diagrams of the form of 2(a) but with the horizontal line replaced by a principal-value integration do not form a geometric series when $m \neq n$. In this work we have omitted continuum interaction resonance energy shifts which are usually quite small.

In the first term of the geometric series we include, in addition to RDI, higher-order diagrams in which the $3d \rightarrow np$ dipole matrix elements are modified by correlations. These diagrams may be separated into two categories. Those in the first

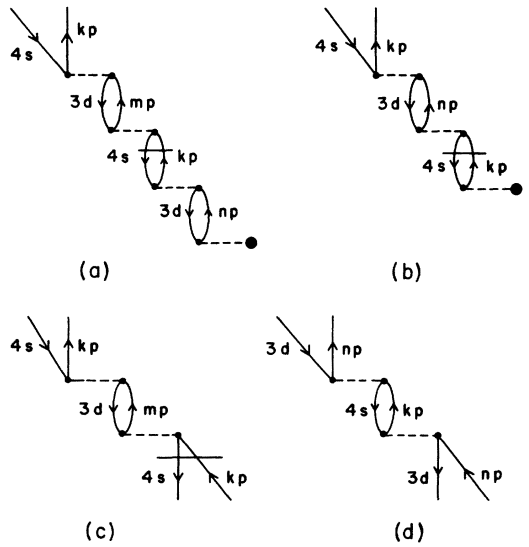

FIG. 2. Diagrams and diagram segments associated with resonances. The horizontal line indicates that the denominator should be treated according to $-i\pi\delta(D)$. The denominator for diagram (d) includes both $\mathrm{P}D^{-1}$ and $-i\pi\delta(D)$.

category have the form given by

$$D_R=\left(\frac{A(p,d)}{A(p,s)}\right)^{1/2}\sum_n\left[\langle\Phi_{kp}|v|\Phi_{np}\rangle M_R(3d\rightarrow np)\right]/D_n, \tag{17}$$

and $M_R(3d\rightarrow np)$ represents any one diagram in the expansion of $Z_R(3d\rightarrow np;\omega)$ which does not include a $4s\rightarrow kp$ excitation with denominator treated according to $-i\pi\delta(D)$ followed (in upward direction) by an even number (including zero) of denominators also treated according to $-i\pi\delta(D)$. The ω dependence of $Z_R(3d\rightarrow np;\omega)$ has been indicated for emphasis. Examples of diagrams represented by $M_R(3d\rightarrow np;\omega)$ are shown in Figs. 1(a)–1(c) with $p,k=3d,np$. Diagram 1(c) with denominator treated according to $-i\pi\delta(D)$ is included except when $q,k'=4s,kp$. This contribution is included in the quantity D_{RT2} defined below. Summing the diagrams in the first category gives

$$D_{RT1}=\left(\frac{A(p,d)}{A(p,s)}\right)^{1/2}\sum_n\left[\langle\Phi_{kp}|v|\Phi_{np}\rangle \times Z_R(3d\rightarrow np;\omega)\right]/D_n(\omega). \tag{18}$$

The second category contains diagrams which include segments excluded from $M_R(3d\rightarrow np)$. These diagrams contribute to

$$D_{RT2}=-i\sum_n\left[\tfrac{1}{2}\Gamma_n(\omega)Z_R^D(4s\rightarrow kp)\right]/D_n(\omega). \tag{19}$$

The lowest-order diagram in this category is shown in Fig. 2(b) with the $4s\rightarrow kp$ dipole matrix element replaced by $Z_R^D(4s\rightarrow kp)$. Higher-order diagrams of this type represent correlation modifications to $\frac{1}{2}\Gamma_n(\omega)$ which have not been considered in this calculation.

It is convenient to introduce the quantity $q_n(\omega)$ defined by Fano in his configuration-interaction theory[21]:

$$q_n(\omega)=Z(3d\rightarrow np;\omega)\left[(2/k)\langle\Phi_{kp}|v|\Phi_{np}\rangle^* \times Z^D(4s\rightarrow kp)\right]^{-1}. \tag{20}$$

Our expression for $q_n(\omega)$ differs from Fano's because his continuum states include a normalization factor $(2/\pi k)^{1/2}$ with respect to ours. In the expressions which follow, the ω dependence will be understood. Writing D_{RT1} in terms of $q_n(\omega)$, we obtain

$$D_{RT1}=\sum_n\left[(\tfrac{1}{2}\Gamma_n)q_nZ_R^D(4s\rightarrow kp)\right]/D_n. \tag{21}$$

Combining D_{RT1} and D_{RT2} and summing the geometric series with ratio R_G, we obtain a total contribution from reduced diagrams having final-state correlations with the resonance configurations

$$D_{RT}=\left[\sum_n\left(\frac{\frac{1}{2}\Gamma_nq_n}{D_n}-\frac{\frac{1}{2}i\Gamma_n}{D_n}\right)\right] \times\left(1+i\sum_m\frac{\frac{1}{2}\Gamma_m}{D_m}\right)^{-1}Z_R^D(4s\rightarrow kp). \tag{22}$$

Finally, combining D_{RT} with the sum of the direct transition diagrams $Z_R^D(4s\rightarrow kp)$, we obtain

$$Z(4s\rightarrow kp)=\left\{\left(1-i\sum_n\frac{\frac{1}{2}\Gamma_n}{D_n}\right)\Big/\left[1+\left(\sum_n\frac{\frac{1}{2}\Gamma_n}{D_n}\right)^2\right]\right\} \times\left(1+\sum_m\frac{\frac{1}{2}\Gamma_mq_m}{D_m}\right)Z^D(4s\rightarrow kp). \tag{23}$$

In Eq. (23) the quantities $Z^D(4s\rightarrow kp)$ and q_m (which involves $Z^D(4s\rightarrow kp)$ and $Z(3d\rightarrow kp;\omega)$) are, in general, complex. However, the imaginary components come from higher-order effects which are usually small and have been neglected in this calculation. In our expansions for $\mathrm{Im}Z_R^D(4s\rightarrow kp)$ and $\mathrm{Im}Z_R(3d\rightarrow np;\omega)$ the lowest-order contributions come from diagrams of the form 1(c) with the denominator for q,k' treated according to $-i\pi\delta(D)$. In our expansion for $Z_R^D(4s\rightarrow kp)$ this diagram with $q,k'=4s,kp$ is canceled by the choice of potential and in the expansion for $Z_R(3d\rightarrow np;\omega)$ it is excluded by definition, and is included in D_{RT2}. Since in this calculation we are only interested in $\omega\langle|E_{3d}|$, there is no contribution from this diagram for excitations with $q=3d$ because then $D(\omega)<0$. It follows that $\mathrm{Im}Z(3d\rightarrow np;\omega)=0$ for this range of ω and similarly, that the lowest-order contribution to $\mathrm{Im}Z^D(4s\rightarrow kp)$ comes from diagram 2(b) with np replaced by kp and kf. This diagram was found to be small and has been neglected. Thus there is good justification in this calculation for considering only the real parts of $Z^D(4s\rightarrow kp)$, $Z(3d\rightarrow np;\omega)$, and $q_n(\omega)$. In the remainder of this paper, these symbols will denote only their real parts. In this approximation, Eq. (23) is equivalent to Fano's configuration-interaction-theory result for the case of many discrete states and one continuum channel.[22] However, one can readily extend the present results by calculating the diagrams which have been omitted.

When the spin-orbit interaction is included in the Hamiltonian, configurations excited by dipole radiation are no longer pure $^1P_1$ states but instead contain admixtures of other LSJ states with $J=1$. In particular, the $^1P_1$, $^3P_1$, and $^3D_1$ states of the $3d^94s^2np$ configurations mix to form intermediate-coupling states

$$|\chi_{nj}\rangle=C_{nj}(^1P)|^1P_1,n\rangle+C_{nj}(^3P)|^3P_1,n\rangle +C_{nj}(^3D)|^3D_1,n\rangle, \tag{24}$$

where n denotes the configuration and j denotes the intermediate-coupled state within a configura-

tion. We extend our expression for $Z(4s \rightarrow kp)$ to include spin-orbit splitting of the resonances by inserting the projection operator $\sum_{nj} |\chi_{nj}\rangle\langle\chi_{nj}|$ into the resonance diagrams discussed above and replacing the energy denominators $D_n(\omega)$ by $D_{nj}(\omega) = E_{3d} - \mathcal{E}_{nj} + \omega$ where $\mathcal{E}_{nj} - E_{3d}$ is the energy of the state χ_{nj} with respect to the ground state and $\mathcal{E}_{nj}$ is found by diagonalizing the intermediate-coupling matrix for HF wave functions. Then we have, instead of D_{RT1},

$$D_{RT1}^{SO} = \left(\frac{A(p,d)}{A(p,s)}\right)^{1/2} \sum_{nj} [\langle \Phi_{kp}|v|\chi_{nj}\rangle\langle\chi_{nj}|\Phi_{np}\rangle \times Z_R(3d \rightarrow np)]/D_{nj} . \tag{25}$$

Using Eqs. (24) and (20), we obtain

$$D_{RT1}^{SO} = \sum_{nj} [|C_{nj}(^1P)|^2 \tfrac{1}{2}\Gamma_n q_n Z_R^D(4s \rightarrow kp)]/D_{nj} . \tag{26}$$

Modifying diagram segments of the form shown in Fig. 2(c) gives the geometric ratio

$$R_G^{SO} = -i \sum_{mj} [|C_{mj}(^1P)|^2 \tfrac{1}{2}\Gamma_m]/D_{mj} . \tag{27}$$

Similarly, modifying the diagrams which contribute to D_{RT2} gives

$$D_{RT2}^{SO} = -i \sum_{nj} |C_{nj}(^1P)|^2 [\tfrac{1}{2}\Gamma_n Z_R^D(4s \rightarrow kp)]/D_{nj} . \tag{28}$$

Finally, when the spin-orbit modified diagrams are combined, we obtain an expression for $Z(4s \rightarrow kp)$ having the same form as the right-hand side of Eq. (23) but with $\sum_n$, $\frac{1}{2}\Gamma_n$, and D_n replaced by $\sum_{nj}$, $\frac{1}{2}\Gamma_{nj} = |C_{nj}(^1P)|^2 \frac{1}{2}\Gamma_n$, and D_{nj}, respectively. This treatment of the spin-orbit split resonances does not include the interaction of the intermediate-coupling states $|\chi_{nj}\rangle$ with the $3d^{10}4skp\ ^3P_1$ continuum channel. The effects of interchannel interactions on resonance line shapes have been discussed by Fano and Cooper[22] and by Mies.[23] We are currently investigating the generalization of our diagrammatic expansion to include these effects.

III. CALCULATIONS AND RESULTS

Bound and continuum orbitals were calculated for the $3d^{10}4skp$, $3d^94s^2kp$, and $3d^94s^2kf$ configurations (k denotes both bound and continuum orbitals) using the potential described above. The Silverstone-Huzinaga potential[24,25] was used when necessary to ensure the orthogonality of excited and occupied orbitals. In order to investigate the effects of core relaxation on $\sigma(\omega)$, we calculated one set of orbitals for the $3d^{10}4skp$ configuration using a frozen-core (FC) potential and another set using an ionic-core (IC) potential. Occupied orbitals of Zn I were used in the FC potential; orbitals of Zn^+ were used in the IC potential. The bound orbitals of the $3d^94s^2np$ configurations were obtained from fully self-consistent HF calculations in order for them to be physically appropriate for the resonances. The continuum orbitals for this configuration were calculated with an IC potential. The $3d^94s^2kf$ orbitals were calculated with a FC potential. When the FC potential is not used, the

TABLE I. Important diagrams[a,b] in the expansion for $Z_R^D(4s \rightarrow kp)$[c].

	Length form			Velocity form		
	k[d]					
Diagrams	0.10	0.30	0.50	0.10	0.30	0.50
1(a)[e]	−1.2066	−1.4091	−0.8676	−0.6813	−0.7578	−0.3992
1(b)[f]	0.1667	0.2322	0.1982	−0.0731	−0.0915	−0.0649
1(b)[g]	0.0485	0.0757	0.0802	−0.3812	−0.5428	−0.4923
1(c)[h]	0.0719	0.1162	0.1332	0.5083	0.7393	0.7016
3(a)	0.2454	0.2453	0.1711	0.1610	0.1233	0.0704
3(b) + 3(c)	−0.0104	−0.0169	−0.0195	−0.0914	−0.1325	−0.1246
other[i]	0.1061	0.1240	0.1303	−0.0171	−0.0992	0.0211
$Z_R^D(rs \rightarrow kp)$	−0.5784	−0.6326	−0.1741	−0.5748	−0.6696	−0.2880

[a] Entries give values of reduced diagrams defined in Sec. II.
[b] Contributions from exchange diagrams are included.
[c] Multiplying entries by $\sqrt{\frac{2}{3}}$ gives contribution to $Z^D(4s \rightarrow kp)$.
[d] $k = [2(\omega - |E_{4s}|)]^{1/2}$, where $|E_{4s}|$ is the ionization energy for a 4s electron.
[e] $p, k = 4s, kp$.
[f] $p, k = 4s, kp$; $q, k' = 4s, np$.
[g] $p, k = 4s, kp$; $q, k' = 3d, kf$.
[h] $p, k = 4s, kp$; $q, k' = 3d, kf$.
[i] Contributions from other diagrams.

excited orbitals are not rigorously orthogonal to ground-state orbitals, however, we found that the overlaps are quite small.

In the following discussion of the diagrammatic expansion of $Z(4s \to kp)$ we will always be referring to the reduced form of the diagrams. The conversion factor $[A(l_k, l_p)]^{1/2}$ between $Z(p \to k)$ and $Z_R(p \to k)$ is understood to be included. This factor equals $\sqrt{\frac{2}{3}}$ and $\sqrt{\frac{4}{3}}$ for $Z(4s \to kp)$ and $Z(3d \to np)$, respectively. Exchange diagrams corresponding to the diagrams shown in the figures will not be discussed but are understood to be included.

In lowest order $Z^D(4s \to kp)$ is given by the HF approximation and is represented by diagram 1(a) with $p, k = 4s, kp$. Values of this diagram near threshold are given in Table I. The corresponding cross section is shown in Fig. 4 for FC orbitals by curves labeled HFL and HFV for length and velocity calculations, respectively. When IC orbitals are used, the L and V forms are increased by 31% and 23%, respectively. The first-order diagrams, which have one interaction with H_c', are shown in Figs. 1(b) and 1(c) with $p, k = 4s, kp$. We used the experimental removal energies[26] $E_{4s} = -0.3452$ a.u. and $E_{3d} = -0.6356$ a.u. We calculated diagram 1(b) for $q, k' = 4s, kp$; $3d, kp$; and $3d, kf$. In calculating diagram 1(c), we included only the continuum part of the $q, k' = 3d, kp$ and $3d, kf$ excitations, according to our prescription for $Z^D(4s \to kp)$, with bound excitations treated separately. Excitations with $q, k' = 4s, kp$ were also omitted due to the choice of potential. The values near threshold of the largest first-order diagrams are given in Table I. As shown in Table I, the dominant correlations in first order involve $4s \to np$ and $3d \to kf$ dipole matrix elements. The L and V forms of diagram 1(b) with $q, k' = 4s, np$ give corrections to lowest order which are roughly equal in magnitude but opposite in sign and which bring $\sigma_L(\omega)$ and $\sigma_V(\omega)$ closer together. The V forms of diagrams 1(b) and 1(c) with $q, k' = 3d, kf$ are very large and are opposite in sign. Their net effect is a reduction of $\sigma_V(\omega)$. The corresponding length diagrams are equal in sign (to each other) but much smaller in magnitude so that these diagrams are less important in the L form than in the V form. These diagrams also reduce $\sigma_L(\omega)$.

The largest higher-order diagram is shown in Fig. 3(a) with $k' = kp$ and kf, and its values near threshold are given in Table I. The diagram of Fig. 3(a) is important because FSC diagrams with $4s \to np$ dipole matrix elements do not occur in lower order and because it has the time ordering which gives the smallest energy denominators. Other diagrams with more than one interaction with H_c' were found to be relatively small. Because of the importance of first-order correlations with $3d \to kf$ velocity dipole matrix elements, we calculated the diagrams shown in Figs. 3(b) and 3(c).

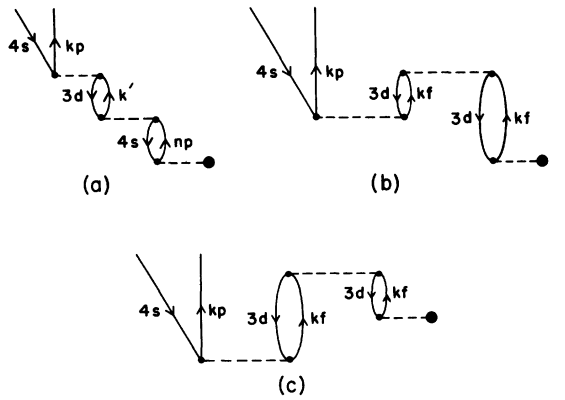

FIG. 3. Important second-order (in H_c') diagrams in the expansion for $Z^D(4s \to kp)$.

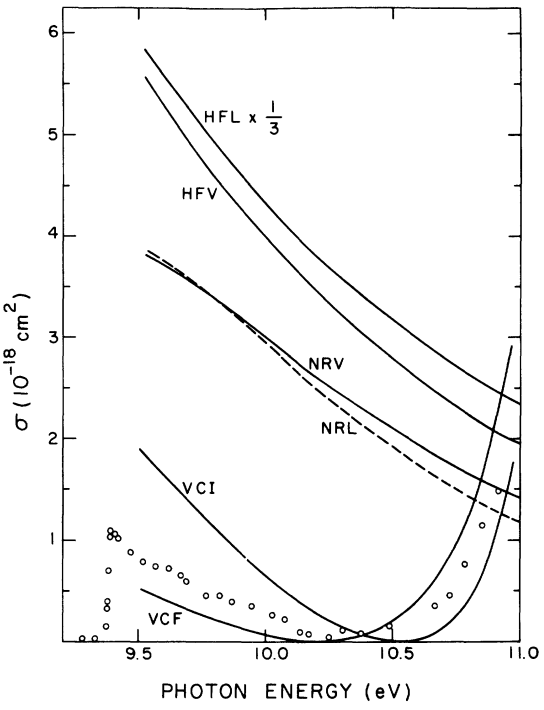

FIG. 4. Cross section $\sigma(\omega)$ for photoionization of the 4s subshell of Zn I near threshold. The curves HFL and HFV represent Hartree-Fock length and velocity cross sections using frozen-core (FC) orbitals. The curves NRL and NRV represent length and velocity cross sections for $Z^D(4s \to kp)$, the correlated direct transition matrix element, with no resonance contributions. The curves VCF and VCI represent correlated (including resonance diagrams) velocity cross sections for $Z(4s \to kp)$ with FC and IC (ionic-core) orbitals respectively. The circles represent experimental data from Ref. 8.

Their values near threshold are also given in Table I. These diagrams increase $\sigma_V(\omega)$ significantly, but have little effect on $\sigma_L(\omega)$. We estimate that a more complete treatment of the RPAE diagrams would lead to changes of less than 20% in our L and V cross sections due to $Z^D(4s \rightarrow kp)$. Our results for the cross section due to $Z^D(4s \rightarrow kp)$ are shown near threshold in Fig. 3 for FC orbitals. The length and velocity curves are denoted by NRL and NRV, respectively. Recall that $Z^D(4s \rightarrow kp)$ omits resonance correlations so that the NRL and NRV curves represent our correlated cross section excluding resonance effects. The corresponding length and velocity IC cross sections are 85% and 64% greater at threshold. Note that the effect of the (nonresonance) correlations included in $Z^D(4s \rightarrow kp)$ is a dramatic reduction in $\sigma_L(\omega)$ but a smaller reduction in $\sigma_V(\omega)$, and it brings them into good agreement. The correlated results shown in Fig. 4 include normalization diagrams described below which reduce the RPAE results by 4%.

In the neighborhood of the $3d^9 4s^2 np$ resonances, $\sigma(\omega)$ depends sensitively on the $3d \rightarrow np$ dipole matrix elements. We find that the correlated matrix elements $Z(3d \rightarrow np; \omega)$ are strongly modified by correlations. We have calculated diagrams 1(b) and 1(c) with $p, k = 3d, np$ and with $q, k' = 4s, kp$; $3d, kp$; and $3d, kf$. For diagram 1(c) the case $q, k' = 3d, kp$ is omitted as it is canceled by the potential.[3] As was found in the calculation of $Z^D(4s \rightarrow kp)$, the largest correlation contributions to $Z(3d \rightarrow np; \omega)$ come from diagrams involving $4s \rightarrow np$ and $3d \rightarrow kf$ dipole matrix elements. In the case of $Z(3d \rightarrow np; \omega)$, however, the $4s \rightarrow np$ correlations are even more dominant, the reason being that $\langle np|z|4s\rangle$ matrix elements are now present in the first-order FSC diagram 1(c). In order to take into account higher-order effects, we used modified $4s \rightarrow np$ dipole matrix elements in the diagrams for $Z(3d \rightarrow np; \omega)$. We find that correlation corrections to the $\langle np|z|4s\rangle$ matrix elements reduce their length and velocity forms for ω near threshold by 22% and 3%, respectively. Table II shows a comparison of correlated and uncorrelated $3d \rightarrow np$ dipole matrix elements for $n = 4-7$. We obtained ω for the correlated values from the average of the resonance energies weighted by $|C_{nj}(^1P)|^2$. Note that the velocity correlated and uncorrelated matrix elements converge faster than the length matrix elements with increasing n. This may indicate that the V form is more reliable.

TABLE II. Comparison of reduced uncorrelated and correlated $3d \rightarrow np$ dipole matrix elements.[a, b]

n	Length form		Velocity form	
	Uncorrelated	Correlated	Uncorrelated	Correlated
4	0.5007	0.7434	0.5433	0.6943
5	0.1433	0.1766	0.1383	0.1558
6	0.0843	0.1002	0.0799	0.0876
7	0.0578	0.0685	0.0546	0.0546

[a] Unreduced matrix elements are obtained by multiplying entries by $[A(p,d)]^{1/2} = \sqrt{4/3}$.

[b] Entries for the correlated matrix elements give values for $Z_R(3d \rightarrow np; \bar{\omega})$ where $\bar{\omega}$ is the average energy of the intermediate-coupling states weighted by $|C_{nj}(^1P)|^2$.

TABLE III. Hartree-Fock data for intermediate-coupling energy matrix[a].

n	$F^2(3d,np)$[b]	$G^1(3d,np)$	$G^3(3d,np)$	ζ_{3d}[c]	ζ_{np}
4	5.304	1.768	1.470	0.500	0.197
5	0.625	0.198	0.168	0.500	0.024
6	0.229	0.074	0.063	0.500	0.009
7	0.111	0.036	0.031	0.500	0.004

[a] Entries are in 10^{-2} a.u.

[b] Direct and exchange Coulomb integrals $F^k(n,n')$ and $G^k(n,n')$ are defined in Ref. 18.

[c] Spin-orbit one-electron integrals are defined in Ref. 29.

The intermediate-coupling energies and mixing coefficients were obtained by the method of Wilson.[27] Electrostatic energy differences between the $^1P_1$, $^3P_1$, and $^3D_1$ multiplets were computed by expressing the differences in terms of average of configuration HF wave functions. The spin-orbit one-electron integrals ζ_{nl} for these wave functions as well as the wave functions themselves were computed using the HF program of C. Froese Fischer.[28] The spin-orbit one-electron integrals are defined by Blume and Watson.[29] The spin-orbit interaction matrix was taken from Condon and Shortley.[30] The data used to construct the intermediate-coupling-energy matrix for $n = 4-7$ is given in Table III. The resonance energies and the squares of the $^1P_1$ mixing coefficients, $C_{nj}(^1P)$, for $n = 4-7$ are given in Table IV. The intermediate-coupling states are labeled by the LS multiplet which mixes in most strongly.

To account for normalization diagrams, we cal-

TABLE IV. Intermediate-coupling resonance energies and $^1P_1$ mixing coefficients.

State[a]	ω_R (a.u.)	$\lvert C_{nj}(^1P)\rvert^2$	State	ω_R (a.u.)	$\lvert C_{nj}(^1P)\rvert^2$
$4p\ ^3P$	0.4105	0.051	$6p\ ^1P$	0.5955	0.569
$4p\ ^1P$	0.4320	0.825	$6p\ ^3P$	0.6075	0.318
$4p\ ^3D$	0.4356	0.124	$6p\ ^3D$	0.6082	0.113
$5p\ ^1P$	0.5640	0.515	$7p\ ^1P$	0.6087	0.585
$5p\ ^3P$	0.5756	0.390	$7p\ ^3P$	0.6210	0.323
$5p\ ^3D$	0.5773	0.095	$7p\ ^3D$	0.6213	0.092

[a] States are labeled by the multiplet with the largest projection.

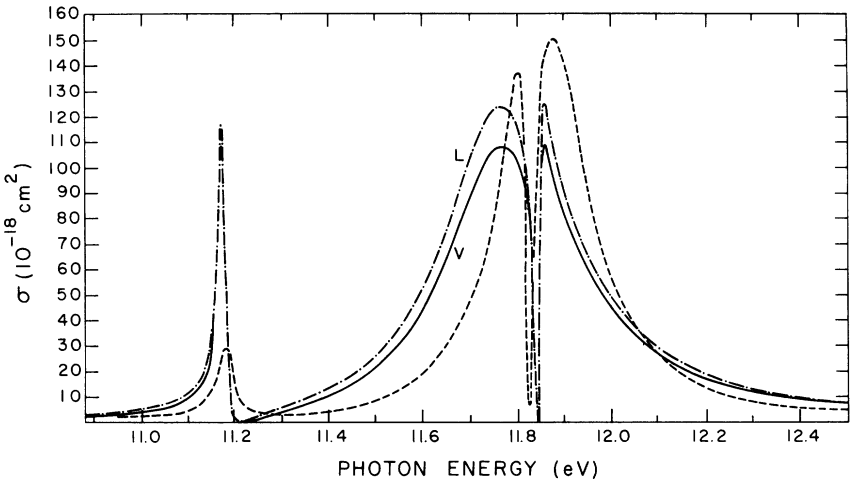

FIG. 5. Cross section $\sigma(\omega)$ in the $3d^9 4s^2 4p$ resonance region. Solid line, correlated velocity cross section; Dash-dot line, correlated length cross section; dashed line, experimental data from Ref. 8.

culated the diagrams shown in Fig. 1(e) (with squared denominator) and its exchange with $q, k' = 4s^-, kp$; $3d, kp$; and $3d, kf$. This gave for the normalization correction factor, $N = 0.96209$.

Our results for $\sigma(\omega)$ calculated from $Z(4s \rightarrow kp)$ including normalization diagrams are shown near threshold in Fig. 4 for the FC and IC velocity forms by the curves labeled VCF and VCI, respectively. The FC and IC length forms lie 10% below and 20% above these curves, respectively. Note that the FC velocity cross section (including resonances), represented by the curve VCF, is strongly reduced from the FC velocity cross section due to $Z^D(4s \rightarrow kp)$ only (resonance diagrams not included) which is shown by the curve NRV. Figure 5 shows the FC length and velocity forms of $\sigma(\omega)$ in the region of the $4p$ resonances. The corresponding IC cross sections are approximately 6% smaller in this region. Figure 6 shows that the FC velocity cross sections for the $n = 5$ and 6 resonances and the $7p\ ^1P_1$ resonance. The oscillator strength f is defined by[1]

$$f = (c/2\pi^2) \int \sigma(\omega)\, d\omega. \tag{29}$$

In Table V our calculated oscillator strengths for the FC velocity resonances are compared with the experimental values of Marr and Austin.[8] Table V and Figs. 4–6 show that most of the oscillator strength for the $4s$ cross section is concentrated in the region of the $4p$ resonances.

We find that there are important interactions between the $3d^9 4s^2 4p$ spin-orbit-split resonances. As shown in Fig. 5, $\sigma(\omega)$ vanishes once between these resonances, creating an absorption window between the two large peaks in agreement with experiment. When the diagrams corresponding to interactions between the resonances are omitted, the absorption window does not occur. However, interactions between the $n = 4$ resonance and $n \geq 5$ resonances and between $n \geq 5$ resonances are quite small. Table VI gives, for $n = 4$–7, the values of

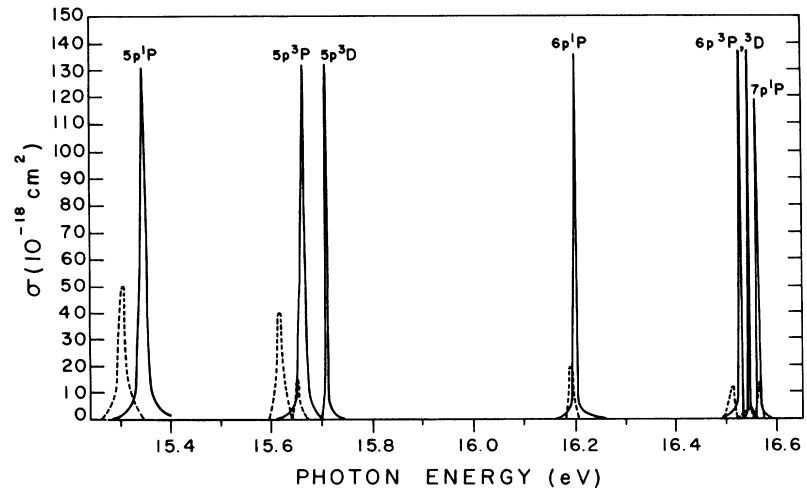

FIG. 6. Cross section $\sigma(\omega)$ in the region of the $3d^9 4s^2 np$ resonances including the $n = 5$ and 6 and the $7p\ ^1P$ resonances. Solid line, frozen-core velocity cross section; dashed line, experimental data from Ref. 8.

$\frac{1}{2}\Gamma_n$ and FC velocity $q_n(\omega)$ and $Z_R^D(4s \rightarrow kp)$ for weighted average (as defined above) resonance energies. Note that the $q_n(\omega)$ change sign after $n=4$. This happens because $Z^D(4s \rightarrow kp)$ changes sign between the $n=4$ and 5 resonances.

IV. DISCUSSION AND CONCLUSIONS

Our calculations indicate that $\sigma(\omega)$ is suppressed near threshold by the presence of the $3d^9 4s^2 4p$ resonances as suggested by Marr and Austin,[8] but we find that other correlation effects are also very important. Reduction of the cross section near threshold due to correlations has also been reported by Amus'ya.[31] Correlations with the $3d^{10}4snp$ and $3d^9 4s^2 kf$ configurations are particularly large as shown in Table I. The fact that the length form of $Z^D(4s \rightarrow kp)$ is most affected by $4s \rightarrow np$ correlations while the V form is most affected by $3d \rightarrow kf$ correlations probably corresponds to the emphasis by the L form on greater distances from the origin compared to the V form. This difference in emphasis may also be responsible for the velocity correlated and uncorrelated $3d \rightarrow np$ dipole matrix elements converging faster than the corresponding length matrix elements. These calculations suggest that the V form of the resonances is more reliable than the L form.

From our investigation of $Z^D(4s \rightarrow kp)$, we find that diagrams with more than one Coulomb interaction are small unless they represent important correlation effects not present in lower order. A good example of this type of diagram is shown in Fig. 3(a) with $k' = kp$ and kf. That is, this is the lowest order in which there is a diagram involving final-state correlations and the large $\langle np|z|4s\rangle$ matrix elements. The good convergence of the diagrammatic expansion is partly the result of the choice of potential which cancels diagrams which are found to be large. We expect that the discrepancy between our FC and IC results for $\sigma(\omega)$ near threshold may be reduced by including diagrams outside the RPAE. We plan to investigate this in future work. From Eq. (23) and including the spin-orbit modifications, we have in the neighborhood of a resonance,

$$\sigma(\omega) \propto \frac{|Z(3d \rightarrow np)|^2}{\frac{1}{2}\Gamma_n}, \quad \omega \approx \omega_R \tag{30}$$

where ω_R is a resonance excitation energy. Equation (30) indicates that the resonance oscillator strengths will be very sensitive to correlation modifications in the quantities $Z(3d \rightarrow np; \omega)$ and $\frac{1}{2}\Gamma_n(\omega)$. It is probable that much of the discrepancy between the calculated and experimental oscillator strengths for $n=4$–7 is due to such modifications. In this calculation we have included only the lowest-order contribution to $\frac{1}{2}\Gamma_n(\omega)$. Marr and Austin[8] have obtained half-widths for the $4p$ resonances by fitting their data to models based on the theoretical studies of Shore[32,33] and Mies.[23] Their results suggest that $\frac{1}{2}\Gamma_4(\bar{\omega})$ may be about 50% larger than our value. We plan in future work to investigate the effect of correlations on $\frac{1}{2}\Gamma_n$. Other correlation effects associated with interactions between the $^1P_1$ and $^3P_1$ continuum channels may also be important.

From the recent analysis of Martin *et al.*,[34] we do not expect the Wilson method to be fully adequate to determine the energy levels and mixing coefficients for the $3d^9 4s^2 4p$ configuration. Therefore, the excellent agreement with experiment obtained for the $n=4$ resonance positions is probably fortuitous. On the other hand, their analysis does indicate that our intermediate-coupling results for $n \geq 5$ are reasonably accurate. Most of the discrepancy in the positions of these resonances is probably due to the electrostatic correlation energy of the $3d^9 4s^2 np$ configurations which we did not include. However, part of the discrepancy is due to our omission of continuum interaction energy shifts.

TABLE V. Comparison between calculated and experimental oscillator strengths.

State	Calculated[a]	Experiment[b]
$4p\ ^3P$	3.75	1.69
^1P / ^3D	41.5[c]	37.8[c]
$5p\ ^1P$	1.75	0.76
^3P	1.23	0.50
^3D	0.34	0.16
$6p\ ^1P$	0.66	0.20
^3P	0.34	0.09
^3D	0.13	0.01
$7p\ ^1P$	0.26	0.15

[a] Results are in units of 10^{-2}.

[b] Experimental oscillator strengths are from Ref. 8 and are given in order of increasing energy.

[c] Entries give sum of oscillator strengths for the two large resonance peaks (labeled ^1P and ^3D in this calculation).

TABLE VI. Resonance parameters for frozen-core velocity cross section.

n	$q_n(\bar{\omega})$[a]	$\Gamma_{(n/2)(\bar{\omega})}$	$Z_R^D(4s \rightarrow kp; \bar{\omega})$
4	12.96	6.352×10^{-3}	0.2025
5	−137.6	0.347×10^{-3}	−0.0284
6	−58.16	0.111×10^{-3}	−0.0725
7	−45.08	0.506×10^{-4}	−0.0893

[a] $\bar{\omega}$ is an average of resonance energies weighted by $|C_{nj}(^1P)|^2$.

Our results show that the absorption window between the $4p\,^1P$ and ^3D resonances is obtained only when interactions between these resonances are correctly included. An important aspect of the experimental data which our treatment does not account for is the variation in the resonance peak heights. As shown by Eq. (30), the diagrams discussed in this work yield roughly constant peak heights. A preliminary investigation indicates that the variation of peak heights is due to interaction between the $^1P_1$ and $^3P_1$ $3d^{10}4skp$ continuum channels.

In addition to the $3d^94s^2np$ resonances (and the $3d^94s^2nf$ resonances which we have omitted), there are also resonances in the 4s cross section due to the excitation of both 4s electrons to excited bound states although these have not been observed. Another interesting correlation effect which begins to contribute slightly above threshold is photoionization accompanied by excitation of a core electron.[35] We intend to study these processes in future work.

ACKNOWLEDGMENT

We wish to thank Professor C. Froese Fischer for the extensive use of her program in this work.

†Work supported by the National Science Foundation.
[1]U. Fano and J. W. Cooper, Rev. Mod. Phys. 40, 441 (1968).
[2]G. V. Marr, *Photoionization Processes in Gases* (Academic, New York, 1967).
[3]M. Ya. Amus'ya, N. A. Cherepkov, and L. V. Chemysheva, Zh. Eksp. Teor. Fiz. 60, 160 (1971) [Sov. Phys.—JETP 33, 90 (1971)].
[4]H. P. Kelly and R. L. Simons, Phys. Rev. Lett. 30, 529 (1973).
[5]A. Dalgarno, H. Doyle, and M. Oppenheimer, Phys. Rev. Lett. 29, 1051 (1972).
[6]G. Wendin, J. Phys. B 6, 42 (1973).
[7]H. P. Kelly and A. Ron, Phys. Rev. A 5, 168 (1972).
[8]G. V. Marr and J. M. Austin, J. Phys. B 2, 168 (1972).
[9]K. A. Brueckner, Phys. Rev. 97, 1353 (1955); and *The Many-Body Problem* (Wiley, New York, 1959).
[10]J. Goldstone, Proc. R. Soc. Lond. A 239, 267 (1957).
[11]H. P. Kelly, Phys. Rev. 131, 684 (1963).
[12]H. P. Kelly, Phys. Rev. 136, 3896 (1964).
[13]H. P. Kelly, Phys. Rev. 144, 39 (1966).
[14]H. P. Kelly, Adv. Theor. Phys. 2, 75 (1968).
[15]H. P. Kelly, Phys. Rev. 182, 84 (1969).
[16]G. Wendin, J. Phys. B 3, 355 (1970); 3, 466 (1970).
[17]D. R. Inglis, Phys. Rev. 38, 862 (1931).
[18]J. C. Slater, *Quantum Theory of Atomic Structure*, Vol. I (McGraw-Hill, New York, 1960), p. 310.
[19]T. Ishihara and R. T. Poe, Phys. Rev. A 6, 111 (1972).
[20]H. P. Kelly, Phys. Rev. A 1, 274 (1970).
[21]U. Fano, Phys. Rev. 124, 1866 (1961).
[22]U. Fano and J. W. Cooper, Phys. Rev. 137, A1364 (1965).
[23]F. H. Mies, Phys. Rev. 175, 164 (1969).
[24]H. J. Silverstone and M. L. Yin, J. Chem. Phys. 49, 2026 (1968).
[25]S. Huzinaga and C. Arnau, Phys. Rev. A 1, 1285 (1970).
[26]C. E. Moore, *Atomic Energy Levels*, Natl. Bur. Std. Circ. No. 467 (U.S. GPO, Washington, D. C., 1949).
[27]M. Wilson, J. Phys. B 1, 736 (1966).
[28]C. Froese Fischer, Comput. Phys. Commun. 1, 151 (1969).
[29]M. Blume and R. E. Watson, Proc. R. Soc. Lond. A 270, 127 (1962).
[30]E. U. Condon and G. H. Shortley, *The Theory of Atomic Spectra* (Cambridge U. P., England, 1935), p. 269.
[31]M. Ya. Amus'ya, in *Proceedings of the Eighth International Conference on the Physics of Electronic and Atomic Collisions* (ICPEAC) edited by B. C. Čubić and M. V. Kurepa (Institute of Physics, Belgrad, Yugoslovia, 1973), p. 171.
[32]B. W. Shore, Rev. Mod. Phys. 39, 449 (1967).
[33]B. W. Shore, J. Opt. Soc. Am. 57, 881 (1967).
[34]W. C. Martin, J. Sugar, and J. L. Tech, J. Opt. Soc. Am. 62, 1488 (1972).
[35]H. P. Kelly, Phys. Rev. A 6, 1048 (1972).